2014 International Conference on Unmanned Aircraft Systems (ICUAS)
May 27-30, 2014. Orlando, FL, USA

Improvement and Validation of a Propeller Slipstream Model for Small Unmanned Aerial Vehicles

Waqas Khan*, and Meyer Nahon, *Member, IEEE*

***Abstract*— Airflow from the propeller, called the propeller slipstream or propwash, plays an important role in the aerodynamics of small unmanned aerial vehicles (UAVs). In fact, flights at low forward speeds or extreme angle of attack (AoA) maneuvers of small fixed-wing UAVs are possible only because the propeller slipstream provides the airflow necessary to maintain lift and control under these conditions. Almost all related works in the literature consider propeller slipstream effect on the UAV's aerodynamics by means of simple theories such as the momentum theory, classical lifting line theory etc. However, these theories take into account only the acceleration of air within the slipstream while failing to account for its diffusion, thereby limiting their applicability to the region near the propeller where acceleration is dominant; far downstream of the propeller, these theories predict unreasonably high induced velocities since diffusion of the slipstream is not accounted for. A propeller slipstream model that considers both acceleration and diffusion within the slipstream has already been presented in a previous work by the authors. The main objective of the current work is to present improvements made to the model in light of detailed experimental measurements of the induced velocity downstream of the propeller. Thereafter, validity of the propeller slipstream model is also demonstrated via additional experiments. The model is shown to be accurate up to an axial distance of ~5 propeller diameters from the propeller plane, with a root mean square error of 0.45 m/s at 1750 rpm and 1.21 m/s at 6425 rpm.**

I. Introduction

Propeller slipstream is one of the key components in modeling aerodynamics for small unmanned aerial vehicles (UAVs) since, being a source of airflow over the control surfaces, it affects the aerodynamic and control forces/ moments, see Fig. 1. This effect can be significant, so much so that it alone can allow the UAV to maintain lift at low forward speeds and allow control of the UAV during high angle of attack maneuvers wherein the external flow is largely detached from the control surfaces. Consequently, flights in constrained environments such as indoors etc., and high angle of attack flights of small UAVs are possible only due to their relatively strong propeller slipstream. Thus detailed knowledge of the induced velocity within the propeller slipstream is essential to accurately determine the aerodynamic and control forces/ moments under these conditions.

Waqas Khan is with the Department of Mechanical Engineering, McGill, Montreal, QC, Canada (phone: +1 514-560-3637; e-mail: waqas.khan@mail.mcgill.ca).

Meyer Nahon is a Professor in the Department of Mechanical Engineering at McGill, Montreal, QC, Canada (email: meyer.nahon@mcgill.ca).

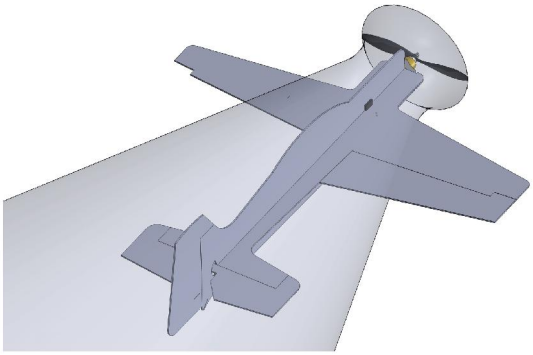

Fig. 1. Propeller slipstream on small propeller-driven UAVs affecting its aerodynamic and control surfaces.

The propeller slipstream effect has been studied in the literature, including some early notable works by George *et al.* [1], McVeigh *et al.* [2], Witkowski *et al.* [3] and Ardito Marretta [4]. More or less, these are iterative methods to predict induced velocity within the slipstream and subsequently the propeller-airframe interaction, based on simple theories such as momentum theory, classical lifting line theory, blade element theory, vortex-lattice method etc. A more recent work on the propeller slipstream is done by Stone [5] for his T-wing tail-sitter UAV. A full azimuthal blade element solution combined with a fixed wake predicts, in real-time, induced velocities over the wing located just behind the propeller. These induced velocities are then used in conjunction with the external flow velocity to calculate the aerodynamic and control forces/ moments. The inherently complex flow field of the propeller slipstream and its even-more-complicated aerodynamic interference with the airframe has led to a large body of experimental work in the literature. Gamble [6], for example, presents detailed experiments to quantify the aerodynamic effect of the propeller slipstream on a micro-air-vehicle's wing, particularly with varying wing position, and rigid vs. flexible wing configurations. Another similar work [7] presents experimentally obtained induced velocity profiles within the propeller slipstream and its effect on the lift and drag coefficients of a micro air vehicle. Computational Fluid Dynamics (CFD) has also been found useful in predicting the complex propeller-airframe interaction [8-9].

As alluded earlier, propeller slipstream models existing in the literature such as those mentioned above are based on simple theories, and as such consider only acceleration occurring within the slipstream, but not diffusion. Therefore their application to regions far downstream of the propeller is questionable, particularly when it is well established that diffusion causes the slipstream to eventually die out far downstream.

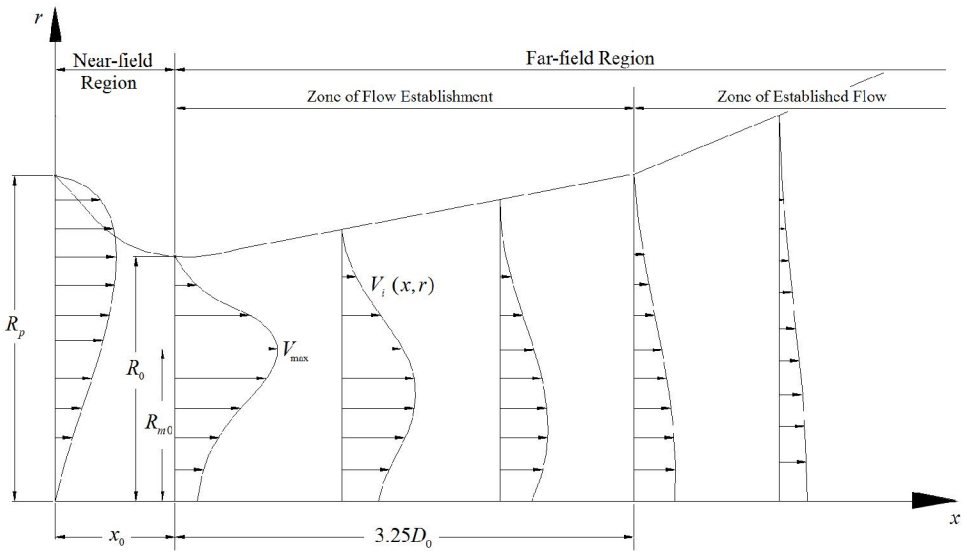

Fig. 2. Detailed propeller slipstream model showing the near-field region, far-field region, zone of flow establishment, zone of established flow, and efflux plane. Also shown is the slipstream contraction up to the efflux plane and the slipstream expansion thereafter.

While the authors have previously presented a propeller slipstream model for small UAVs [10] that takes into account both acceleration and diffusion phenomena using simple analytical and semi-empirical equations, the objective of the current work is to present improvements made to the slipstream model in light of detailed experimental measurements of the induced velocity within the slipstream. The validity of the proposed model is also demonstrated in the current work through comparison with additional experiments.

II. Propeller Slipstream Model

Prior to presenting the improvements made to the propeller slipstream model, it is first necessary to briefly describe the original model given in [10].

A. Evolution of the Propeller Slipstream

Acceleration and diffusion are two major phenomena that occur within the slipstream. The pressure force associated with the rotating propeller causes the air passing through it, to accelerate in all three directions i.e. axial, tangential and radial. Of these, acceleration in the axial direction is dominant and the only one considered in the current work. As a result of acceleration, the induced air velocity within the slipstream increases, while the slipstream itself contracts to preserve continuity. On the other hand, air viscosity and turbulence cause diffusion of the slipstream laterally into the ambient flow. Induced air velocity within the slipstream decreases as a result of momentum transfer from the fast-moving slipstream to the slow-moving ambient flow, and is accompanied by expansion of the slipstream for continuity.

In reality, the aforementioned phenomena of acceleration and diffusion coexist within the propeller slipstream, however their relative importance is key to determining whether the slipstream will contract or expand. Since near the rotating propeller, the pressure force is stronger than the viscous force, acceleration dominates diffusion and therefore, contraction occurs near the propeller, as suggested by the classical momentum theory. However, the influence of this pressure force diminishes as the air moves downstream, and at some distance downstream, the pressure force becomes weaker than the viscous force and turbulence. Then diffusion dominates causing the slipstream to expand from that point onwards.

B. Propeller Slipstream Model

The propeller slipstream model is developed by identifying two distinct regions within the slipstream namely near-field region and far-field region as shown in Fig. 2.

In the near-field region, only acceleration within the slipstream is considered, neglecting diffusion. The region is therefore characterized by contraction of the slipstream. Simple theories, such as momentum theory, hold valid and are used to predict induced velocity in this region. By contrast, only diffusion is considered in the far-field region that causes slipstream expansion. However, analyzing diffusion, even alone, by treating air as viscous and turbulent in this region is not trivial. No simple analytical equations exist in the literature for this purpose and therefore, semi-empirical equations, originally developed for marine propeller jets, are used here to predict induced velocity in this region of the slipstream.

A transition plane located at an axial distance x_0 separates the two regions and is termed as the efflux plane. Upstream of this plane, the slipstream contracts becoming narrowest at the efflux plane and expands thereafter, see Fig. 2. The induced velocity increases starting from the propeller plane in the near-field region, becomes a maximum at the efflux plane, and then decreases downstream until it equals the ambient flow velocity. The momentum-averaged induced velocity at the efflux plane is termed as the efflux velocity V_0, and the smallest radius there is termed as the contracted radius R_0.

Before proceeding further, some description of the far-field region is also necessary. It is well established from research on marine propeller jets, that the far-field region comprises of two distinct zones namely the Zone of Flow Establishment (ZFE) and the Zone of Established Flow (ZEF) as shown in Fig. 2. The ZFE is characterized by two maximum induced velocity peaks, one on either side of propeller rotation axis (only one peak is shown in Fig. 2 since flow is axisymmetric about the rotation axis). These peaks gradually move inward toward the rotation axis. A certain distance downstream, these two peaks merge into a single induced velocity peak located at the rotation axis, marking the beginning of the ZFE. Thereafter, the induced velocity decreases in the ZFE as the slipstream diffuses outwards until it is no longer distinguishable from the ambient flow.

A table in [10] summarizes all the analytical and semi-empirical equations that constitute the propeller slipstream model.

III. Improvements to the Propeller Slipstream Model

This section presents the improvements made to the propeller slipstream model in [10], in light of detailed measurements of induced velocity within the slipstream. Only the far-field region is targeted for improvement in this paper, since classical momentum theory is well-known to yield adequate results in the near-field region of the slipstream. The experimental setup and procedure are discussed first, followed by a description of the improvements made to the model.

A. Experimental Setup and Procedure

The experimental setup consists of a test propeller: an *APC 10X4.7* (0.254m diameter) – a commonly used propeller on small UAVs, attached to a brushless dc motor. As shown in Fig. 3, the assembly is mounted on a stand firmly attached to an ATI Gamma force/torque (F/T) transducer, to measure the thrust generated by the propeller. The stand keeps the propeller clear from the ground to avoid any interference between the propeller slipstream and the surroundings.

Three sets of experiments were performed each at a different rotational speed: low (1750 rpm), moderate (5425 rpm) and high (6425 rpm). An Arduino board was used to send PW signals to the motor-propeller assembly to run it at the desired rotational speed, while the induced velocity was measured downstream of the propeller at several axial and radial locations using a handheld *Reed* hot-wire anemometer which has a sampling rate of 1 Hz, and a resolution of 0.01 m/s in the range 0.2 – 5 m/s, and 0.1 m/s in the range 5.1 – 25 m/s. The mechanical setup shown in Fig. 3 was designed so that the hot-wire anemometer could be traversed in the axial as well as radial direction within the propeller slipstream.

Keeping in view our interest in the far-field region only, axial locations were selected downstream of the efflux plane i.e. $x > x_0$. The location of efflux plane was determined by the analytical equation presented in [10], and was found to be around $x_0 = 195$ mm for the test propeller. Therefore, the measurement grid was established at axial locations $x = [220,\ 300,\ 400,\ 500,\ 700,\ 900,\ 1100,\ 1300]$ mm measured from the propeller plane, and at radial locations $r = 0$ to 370 mm at 10 mm intervals measured from the rotation axis.

B. Improvements to the Propeller Slipstream Model

Based on one set of experiments, performed at 5425 rpm and a recent work by Lam [11], the following improvements are made to the original propeller slipstream model.

1) Efflux Velocity and Contracted Radius

Previously, the efflux velocity was calculated using the semi-empirical equation: $V_o = 1.33 n D_p \sqrt{C_t}$ where n is the rotational speed of the propeller in rev/s, D_p is the propeller diameter, and $C_t = T \Big/ \left(\rho n^2 D_p^{\,4} \right)$ is the thrust coefficient. The equation was proposed by Hamill [12] based on his

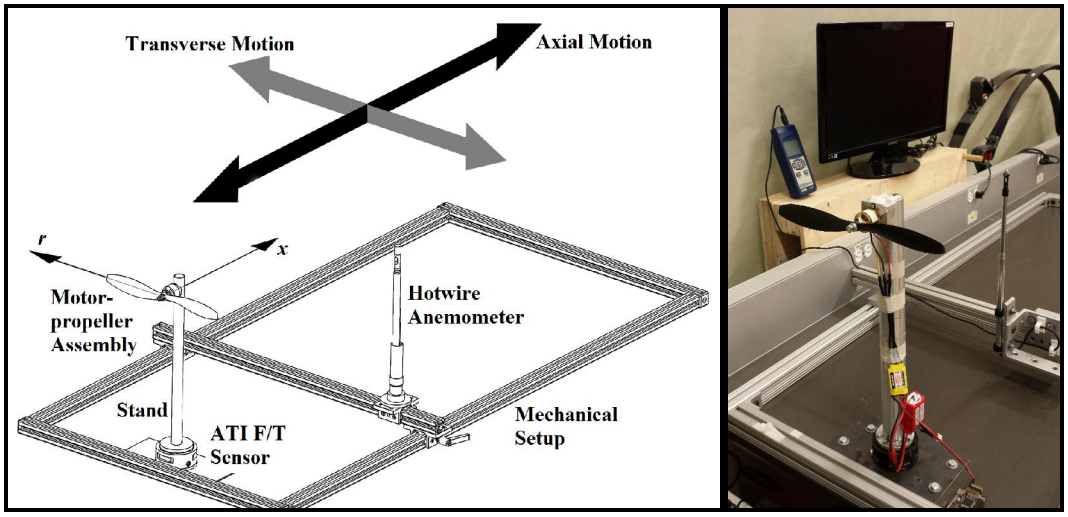

Fig. 3. Experimental setup for the measurement of induced velocity at a number of axial and radial locations behind the propeller.

experiments of marine propeller jets, which suggested a lower coefficient (1.33) compared to that predicted by momentum theory (1.59). From a recent experimental work by Lam [11], Hamill's equation clearly under-predicts the efflux velocity by as much as ~22% from experimental results. Therefore, to improve the propeller slipstream model, Hamill's equation is replaced by a semi-empirical equation given by Hashmi [13]:

$$V_o = E_o n D_p \sqrt{C_t} \tag{1}$$

where the coefficient $E_o = (D_p / D_h)^{-0.403} C_t^{-1.79} \sigma^{0.744}$ is not constant but rather depends on the propeller characteristics such as propeller hub diameter D_h and solidity ratio σ (projected area of all blades divided by the propeller disc area). Besides being propeller dependent, Hashmi's equation is also shown to have a better correspondence with experimental results (~10%) [11].

2) Semi-Empirical Coefficients

Diffusion in the far-field region is taken into account via semi-empirical equations that were developed for marine propeller jets. Their use for an aircraft propeller slipstream is justified considering that the flow is incompressible in both cases and more so, density of the fluid is explicitly considered as a parameter in the equations. However, since viscosity of the fluid is not considered explicitly in the semi-empirical equations, the experimentally determined coefficients (that represent quantities such as the rate of decay of the maximum induced velocity etc.) may be different for an aircraft propeller slipstream. Therefore, a major improvement to the existing propeller slipstream model is the correction of these coefficients for a propeller slipstream in air from a set of experimental measurements.

Semi-empirical equations developed by Stewart [14] for marine propellers were used to predict the maximum induced velocity at each cross-sectional plane in both zones of the far-field region. Fig. 4 shows experimentally measured values for the maximum induced velocity versus those predicted by Stewart's equations (dotted lines). Clearly, the experiments show a slower decay of maximum induced velocity with axial distance. This is expected since air has a higher kinematic viscosity than water causing relatively less viscous shearing within the propeller slipstream and therefore lower lateral diffusion into ambient flow. A primitive attempt was made in the previous work [10] to cater for the different kinematic viscosities of water and air. However, in the current work, the coefficients in Stewart's equations are corrected by curve-fitting experimentally measured maximum induced velocity, leading to the modified Stewart's equations below.

$$V_{\mathrm{ZFE\,max}} = V_0 \left[1.260 - 0.1047 \left(x - x_0 \right) / D_0 \right] \tag{2}$$

$$V_{\mathrm{ZEF\,max}} = V_0 \left[0.973 - 0.0534 \left(x - x_0 \right) / D_0 \right] \tag{3}$$

where $D_0 = 2R_0$ is the contracted diameter. Maximum induced velocities predicted by the modified Stewart's equations are also shown in Fig. 4 with solid lines.

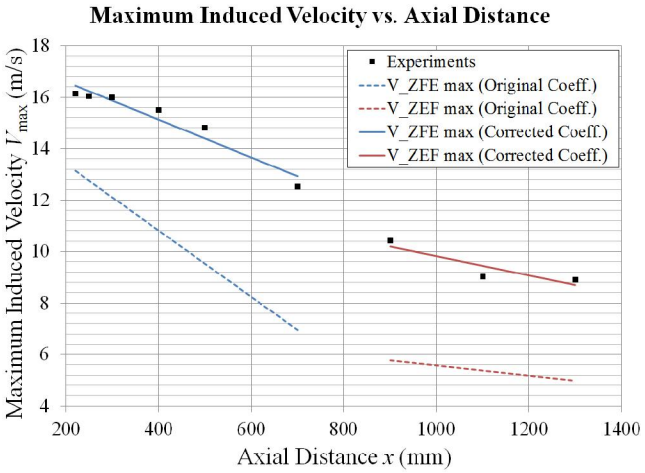

Fig. 4. Experimentally measured maximum induced velocities versus simulated values (dotted lines) using original Stewart's semi-empirical equations. Also shown are predicted values (solid lines) using modified Stewart's equations.

Similarly, coefficients in the semi-empirical equations for induced velocity profiles are corrected using experimentally measured profiles at a few axial locations (one axial location in each zone of the far-field region), as shown in Fig. 5. The modified semi-empirical equations obtained thereof are,

For $x_0 \le x \le (x_0 + 0.5D_0)$:

$$V_i(x,r) = V_{\mathrm{ZFE\,max}} \mathrm{e}^{-0.3\left(\frac{r - R_{m0}}{0.5 R_{m0}} \right)^2} \tag{4}$$

For $(x_0 + 0.5D_0) < x \le (x_0 + 3.25D_0)$:

$$V_i(x,r) = V_{\mathrm{ZFE\,max}} \mathrm{e}^{-0.35\left(\frac{r - R_{m0}}{0.5R_{m0} + 0.075(x - x_0 - R_0)} \right)^2} \tag{5}$$

For $x > (x_0 + 3.25D_0)$:

$$V_i(x,r) = V_{\mathrm{ZEF\,max}} \mathrm{e}^{-15.2\left(\frac{r}{x - x_0} \right)^2} \tag{6}$$

where $R_{m0} = 0.7\left(R_p - R_h \right)$ represents the location of maximum induced velocity at the efflux plane. A summary of all improvements made to the propeller slipstream model is given in Table I.

IV. Validation

The improved propeller slipstream model is validated against *other* sets of experiments. As stated in Section III A, three different sets of experiments were performed at 1750 rpm, 5425 rpm and 6425 rpm respectively. While, in the previous section, one set of these experiments (done at 5425 rpm) was used to correct semi-empirical coefficients, the other two sets of experiments (done at 1750 rpm and 6425 rpm) are used here for validation of the improved propeller slipstream model.

A qualitative comparison of the entire propeller slipstream is shown in Fig. 6(a) and Fig. 6(b) for 1750 rpm and 6425 rpm respectively. The plotted induced velocities

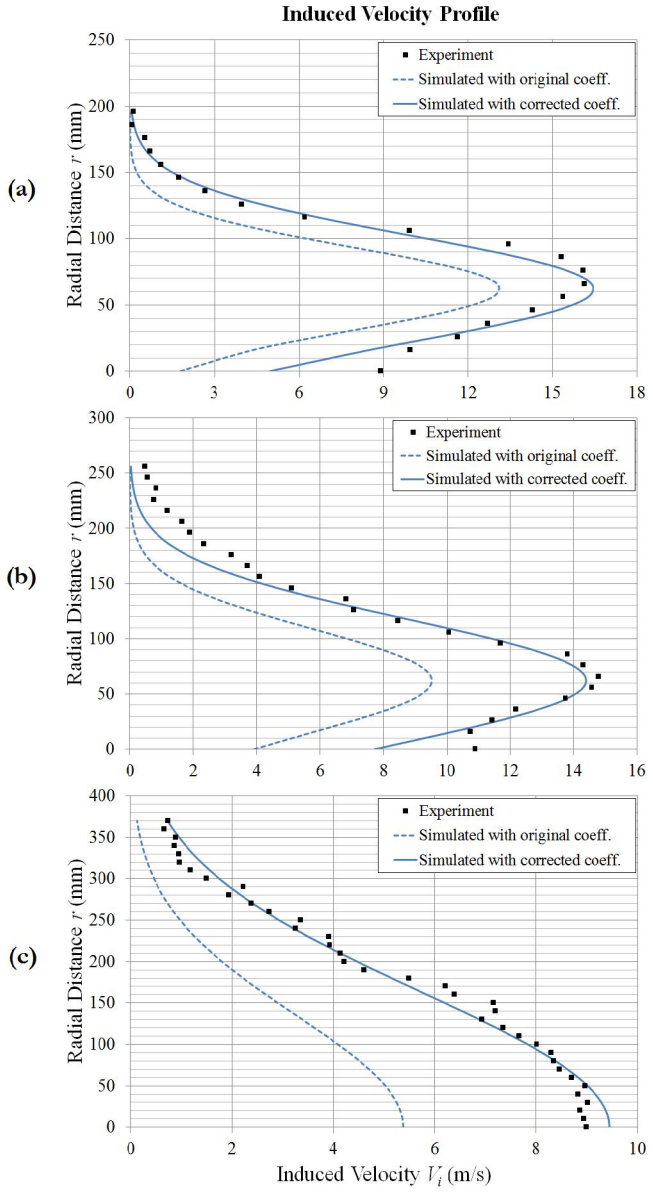

Fig. 5. Comparison of experimentally measured induced velocity profiles with those predicted using original semi-empirical equations (at 5425 rpm) at axial locations (a) x = 220mm (b) x = 500 mm and (c) x = 1100mm. Induced velocity profiles predicted using modified semi-empirical equations (4), (5) and (6) are also shown with solid lines.

are not actual values but are scaled (by a factor of 5 in Fig. 6(a) and 1.8 in Fig. 6(b)) to fit the grid for qualitative comparison only. A quantitative comparison is also shown at axial locations x = 400 mm (left) and 1100 mm (right) in Fig. 6(c). Actual values of the induced velocities are plotted on the x-axis with radial distance on the y-axis. A good match is seen between experiments and simulation, thereby validating the propeller slipstream model in general and the corrected coefficients in particular. Table II lists the root mean square (rms) error in induced velocity at each axial location. The overall rms error is found to be 0.45 m/s at 1750 rpm, and 1.21 m/s at 6425 rpm.

TABLE I. SUMMARY OF IMPROVEMENTS TO THE SLIPSTREAM MODEL

Semi-Empirical Equations	Coefficients		
		Orig. Value	*Corr. Value*
$V_o = \mathbf{a_1} n D_p \sqrt{C_t}$	a_1	1.33	E_0
$V_{ZFE\max} = V_0\left[\mathbf{a_2} - \mathbf{b_2}\left(x - x_0\right)/D_0\right]$	a_2 b_2	1.0172 0.1835	1.260 0.1047
$V_{ZEF\max} = V_0\left[\mathbf{a_3} - \mathbf{b_3}\left(x - x_0\right)/D_0\right]$	a_3 b_3	0.543 0.0281	0.973 0.0534
$V_i(x,r) = V_{ZFE\max} e^{-\mathbf{a_4}\left(\frac{r-R_{m0}}{0.5R_{m0}}\right)^2}$	a_4	0.5	0.3
$V_i(x,r) = V_{ZFE\max} e^{-\mathbf{a_5}\left(\frac{r-R_{m0}}{0.5R_{m0}+0.075(x-x_0-R_0)}\right)^2}$	a_5	0.5	0.35
$V_i(x,r) = V_{ZEF\max} e^{-\mathbf{a_6}\left(\frac{r}{x-x_0}\right)^2}$	a_6	22.2	15.2

Near the propeller hub, the simulation under-predicts induced velocity at both rotational speeds as shown in Fig. 6(c). However, this under-prediction decreases with axial distance, with no under-prediction at large axial distances. This can be explained by noting that the semi-empirical equations assume a large ship propeller hub that reduces the induced velocity at the center significantly [11], while on the other hand, small UAV propellers have a small hub causing less reduction in induced velocity at the core. It must also be realized that in reality, induced velocity at the center is of lesser importance because of the aircraft fuselage there. If the near-hub region i.e. r = 0 mm is not taken into account, the rms error improves to 0.4 m/s at 1750 rpm and 0.88 m/s at 6425 rpm, indicating clearly that much of the error is due to the hub issue explained above.

TABLE II. ROOT MEAN SQUARE ERROR IN INDUCED VELOCITY

Axial Distance x (mm)	RMS Error (m/s) 1750 RPM	RMS Error (m/s) 6425 RPM
220	0.55	1.5
250	0.54	1.54
300	0.54	2.14
400	0.48	1.29
500	0.37	1.10
700	0.36	0.68
900	0.51	1.17
1100	0.38	0.38
Overall RMS error	**0.45**	**1.21**
RMS error excluding hub	**0.4**	**0.88**

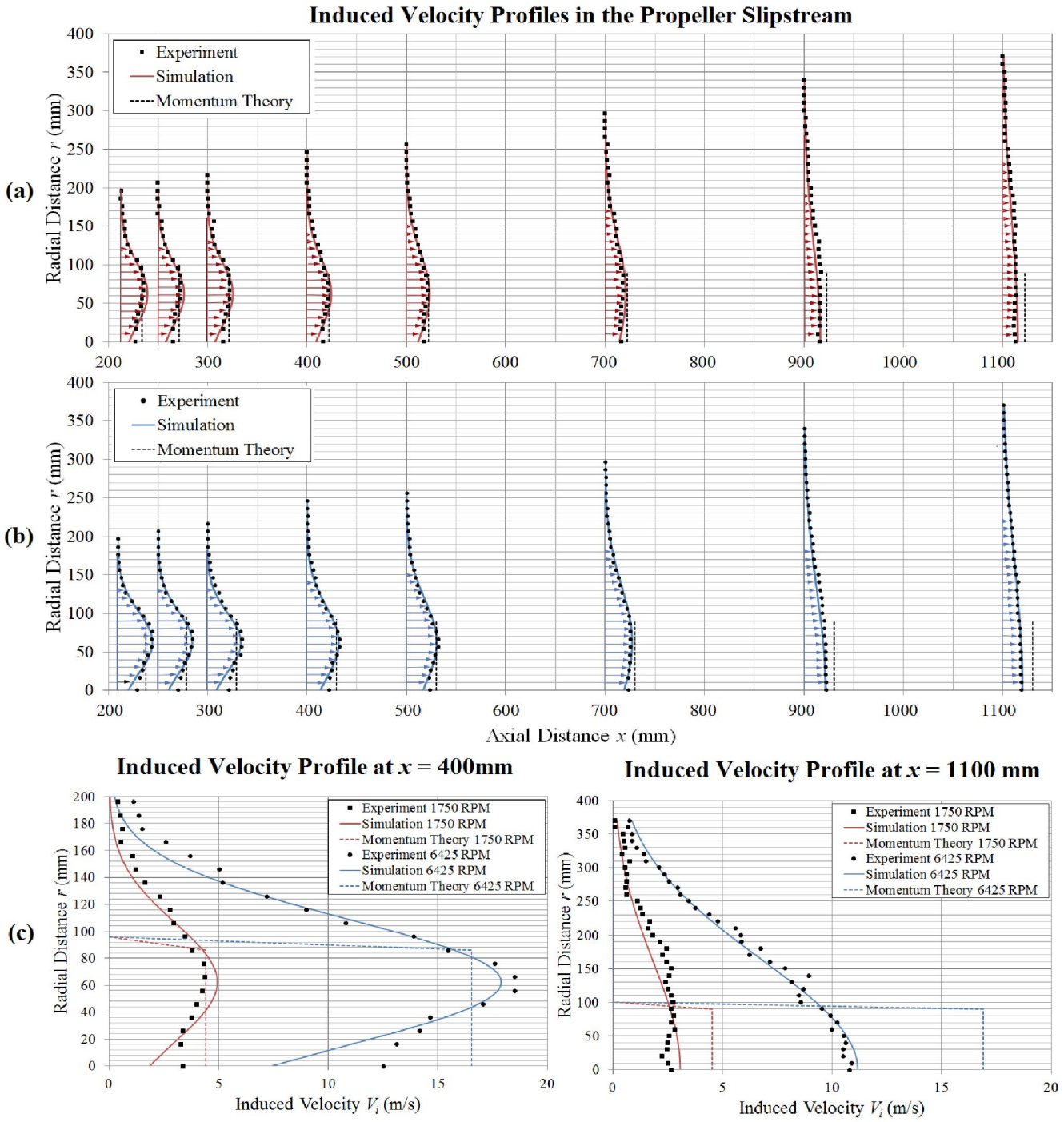

Fig. 6. Plot showing a good qualitative agreement between experimental and simulated induced velocity profiles within the propeller slipstream at (a) 1750 rpm and (b) 6425 rpm. The induced velocity is scaled by a factor of 5 in (a) and by 1.8 in (b) to fit the grid*. For quantitative comparison, actual values of the induced velocity are plotted in (c) at x = 400 mm (left) and 1100 mm (right). Average induced velocities from momentum theory are also plotted up to their respective slipstream radii (predicted also by momentum theory). Outside of the slipstream radii, the theory predicts zero induced velocity.

*Length of velocity arrow (in mm) = Scale factor X Magnitude of velocity (in m/s)

Also plotted in Fig. 6 is the average induced velocity obtained using the widely-used momentum theory. The average induced velocity is plotted up to slipstream radius predicted by momentum theory itself; outside of this slipstream radius, the theory predicts a zero induced velocity as shown in Fig. 6. Discrepancy between the momentum theory predictions and experimental results with increasing axial distance is evident. Obviously, this is due to the diffusion of the slipstream that momentum theory does not account for. Plotting momentum theory predictions in Fig. 6 highlights the severity of diffusion in the far-field region of the slipstream, as well as the need for a propeller slipstream model, such as the one presented in this paper, which accounts for it.

V. CONCLUSION

The research presented in this paper focused on improvements of a propeller slipstream model capable of taking into account both acceleration and diffusion within the slipstream. Improvements were targeted at the far-field region of the slipstream that was previously defined by semi-empirical equations developed for marine propeller jets. Relevant semi-empirical coefficients were corrected for an aircraft slipstream in air using detailed experimental measurements of the induced velocity. Finally, the improved model was validated against additional experiments, demonstrating excellent match between the two with an rms error of 0.45 m/s at 1750 rpm and 1.21 m/s at 6425 rpm. The model was validated up to an axial distance of ~5 propeller diameters downstream, and is thus suitable for most small sized UAVs. In future, the effect of advance ratio on the slipstream will be studied in detail in a wind-tunnel to devise a simple approach to account for that effect. More experimental validation will also be carried out with different test propellers.

REFERENCES

[1] M. George and E. Kisielowski, "Investigation of propeller slipstream effects on wing performance," TRECOM Technical Report 67-67, U.S. Army Aviation Materiel Laboratories, Fort Eustus, Virginia, 1967.

[2] M. A. McVeigh, L. Gary, and E. Kisielowski, "Prediction of span loading of straight-wing/ propeller combinations up to stall," NASA CR-2602, 1975.

[3] D. P. Witkowski, A. K. H. Lee, and J. P. Sullivan, "Aerodynamic interaction between propeller and wings," Journal of Aircraft, vol. 26, no. 9, pp. 829-836, 1989.

[4] R. M. Ardito Marretta, "Different wing flowfields interaction on the wing-propeller coupling," *Journal of Aircraft*, vol. 34, no. 6, pp. 740-747, 1997.

[5] R. H. Stone, "Aerodynamic modeling of the wing-propeller interaction for a tail-sitter unmanned aerial vehicle," *Journal of Aircraft*, vol. 45, no. 1, pp. 198-210, 2008.

[6] B. J. Gamble, "Experimental analysis of propeller interactions with a flexible wing micro-air-vehicle," M. S. Thesis, Dept. of Aeronautics and Astronautics, Air Force Institute of Technology, Wright-Patterson AirForce Base, OH, 2006.

[7] S. Shkarayev, J. Moschetta, and B. Bataille, "Aerodynamic design of micro air vehicles for vertical flight," *Journal of Aircraft*, vol. 45, no. 5, pp. 1715-1724, 2008.

[8] E. W. M. Roosenboom, A. Sturmer, and A. Schroder, "Advanced experimental and numerical validation and analysis of propeller slipstream flows," *Journal of Aircraft*, vol. 47, no. 1, pp. 284-291, 2010.

[9] W. Fu, J. Li, and H. Wang, "Numerical simulation of propeller slipstream effect on a propeller-driven unmanned aerial vehicle," International conference on Advances in Computational Modeling and Simulation, *Procedia Engineering* 31, pp. 150-155, 2012.

[10] W. Khan, R. Caverly, and M. Nahon, "Propeller slipstream model for small unmanned aerial vehicles," AIAA 2013-4907, Boston, MA, August 2013.

[11] W. Lam, G. Hamill, D. Robinson, S. Raghunathan, and Y. Song, "Analysis of the 3D zone of flow establishment from a ship's propeller," *KSCE Journal of Civil Engineering*, vol. 16, no. 4, pp. 465-477, 2012.

[12] G. A. Hamill, "Characteristics of the screw wash of a manoeuvring ship and the resulting bed scour," PhD Thesis, The Queen's University of Belfast, Northern Ireland, 1993.

[13] H. N. Hashmi, "Erosion of a granular bed at a quay wall by a ship's screw wash," PhD Thesis, The Queen's University of Belfast, Northern Ireland, 1993.

[14] D. P. J. Stewart, G. A. Hamill, and H. T. Johnston, "Velocities in a ship's propeller wash," Proc. of Internation Symposium on Environmental Hydraulics, Rotterdam, 1991.